

Fast magnetosonic waves launched by transient, current sheet reconnection

D. W. Longcope

Department of Physics, Montana State University, Bozeman, Montana 59717, USA

E. R. Priest

*Department of Mathematics and Statistics, University of St. Andrews,
St. Andrews KY16 9SS, United Kingdom*

(Received 6 September 2007; accepted 12 November 2007; published online 18 December 2007)

A model is investigated describing the resistive dissipation of a finite, two-dimensional current sheet subject to suddenly enhanced resistivity. The resistivity rapidly diffuses the current to a distance where it couples to fast magnetosonic modes. The current then propagates away as a sheath moving at the local Alfvén speed. A current density peak remains at the X-point producing a steady electric field independent of the resistivity. This transfers flux across the separatrix at a rate consistent with the external wave propagation. The majority of the magnetic energy stored by the initial current sheet is converted into kinetic energy, far from the reconnection site, during the fast mode propagation. © 2007 American Institute of Physics. [DOI: 10.1063/1.2823023]

I. INTRODUCTION

The first models of magnetic reconnection were of a steady-state process occurring at a magnetic neutral point, or X-point.^{1–4} An electric field at the X-point transfers magnetic flux and converts magnetic energy to both heat and kinetic energy. The structure of magnetic reconnection in these models has been largely borne out by subsequent investigation.

A notable shortcoming of these steady-state models is in illuminating the energetics of magnetic reconnection. For example, they involve a velocity field extending to arbitrarily large distances, so kinetic energy is potentially infinite. It is therefore difficult to identify the source of the kinetic energy in order to discriminate between flow generated by the reconnection itself (spontaneous reconnection) or due to an external agent “driving” the reconnection (forced reconnection). In Petschek’s model and its generalizations by Priest and Forbes,⁵ the bulk of the energy conversion is not in the diffusion region, but rather at the four standing slow-mode shock waves extending from it. In this paper, we shall suggest a possible source for this energy, which in the above models is simply assumed to be stored throughout space and brought in by a steady flow.

The energetics of reconnection are more readily studied in models of transient reconnection episodes, with a definite beginning. Semenov *et al.*⁶ and then Biernat *et al.*⁷ studied the effects of a sudden localized reconnection event occurring on an existing current sheet. In their models, and subsequent developments,^{8,9} an infinite current sheet separates two layers of uniform magnetic field. A localized electric field, perhaps due to an enhancement in resistivity, is introduced beginning at time $t=0$ at a single point in the sheet. This creates an X-point at that particular point and causes shocks of various characters—fast, slow, and intermediate—to propagate outward.

In a later study of a similar model, Nitta *et al.*^{10,11} considered a reconnection electric field that persisted at a constant value after its introduction at $t=0$. They found a self-similar solution in which a circular fast magnetosonic (FMS)

shock establishes, in its wake, reconnection inflow and outflow matching a more traditional steady-state reconnection at the X-point, including slow shocks emanating from the X-point. The fast mode changes the magnetic field only slightly so the slow shocks make a small angle with the current sheet, as in Petschek’s steady-state model.

The structure of the reconnection at the X-point strongly resembled the steady-state solutions, even though these models were decidedly unsteady.¹² The unsteady models did, however, reveal a novel energy release scenario. As the shocks of each type expand away from the reconnection site, they convert magnetic energy into heat and kinetic energy. A vanishing fraction of this energy conversion occurs within the reconnection site itself, which is, after all, very small. The energy conversion is therefore a more global process than steady-state theories suggest. Significant energy is converted not only at standing slow-mode shocks but also at outward-propagating fast-mode shocks.

Models with infinite current sheets do, however, possess artifacts in their energetics. The infinite sheet is intended to represent only a small piece of a realistic, finite current sheet. Thus the shocks become less realistic by the time they leave the local neighborhood. A finite current sheet creates a magnetic field diminishing inversely with distance, rather than indefinitely uniform. The extended magnetic field created by a local sheet is the free energy that reconnection will tap. Reconnection will diminish the current, thereby decreasing the energy in the extended field. In uniform models with infinite sheets, on the other hand, neither their net current nor their far field are significantly changed by reconnection. Finite sheets are thus uniquely suited to reveal an essential element of reconnection energetics: A local, diffusive process (reconnection) must initiate global energy release.

In models of two-dimensional, transient reconnection, we expect the X-point to play two different roles at once. As in other models, an X-point will form within the sheet at the reconnection site. A global X-point is also the field structure within which the finite current sheet is most naturally em-

bedded. This is a by-product of the X-point's tendency to "collapse" under slow, external perturbation, creating the current sheet in the first place.¹³⁻¹⁵ In the absence of reconnection, these current sheets are associated with "storage," as magnetic energy, of the work done by the slow perturbations. (The current sheet is finite but the field it creates extends throughout space, and this is where the energy is actually stored.) Changes to the current sheet produced locally by transient reconnection, especially the change in net current, must propagate outward along the global X-point field in which the sheet finds itself. The details of this propagation differ from models with infinite sheets, since those are embedded in a uniform external field.

Fast modes in the vicinity of an X-point were studied by Craig and McClymont¹⁶ and Hassam¹⁷ (hereafter they will be collectively referred to as CMH). In order to focus on the interaction of dissipation with wave propagation, they studied dynamics in the absence of plasma pressure. A cylindrical disturbance was initiated at some distance from an initially current-free X-point. The disturbance converged from every direction toward the X-point where the diffusive effects of resistivity become significant. Only at this point is some of the current and energy of the disturbance dissipated. The disturbance is also reflected by this dissipation and propagates outward beyond further effects of diffusion. If it is reflected once more at the outer boundary, the process will repeat with subsequent dissipation and reflection.

Both studies found that the energy of the disturbance was largely dissipated after several bounces. This corresponds to the Alfvén transit time multiplied by the squared logarithm of the Lundquist number at the boundary (i.e., proportional to the squared logarithm of the inverse resistivity). The energy dissipation in this model is therefore fast since it depends only very weakly on the value of diffusivity. Following the above discussion, it is also significant that dissipation is almost entirely localized to the X-point itself.

In the present study, we use the CMH model^{16,17} to study the outward propagation of fast mode disturbances initiated by reconnection at the X-point itself. This will provide insight into the energy release initiated by reconnection. No matter how the reconnection occurs, it will be localized to a region near the current sheet, and therefore near the X-point. It will transfer flux through the X-point, thereby seeking to reduce the current in the sheet itself. This change has implications at arbitrary distances where the magnetic field is proportional to that current.

The adjustment of distant field by fast waves constitutes energy release. Its remoteness from the initial current sheet makes it unlikely that the energy release will depend on details of the reconnection process. In the interest of simplicity, therefore, we choose a very simple model of a transient reconnection process. In our model, the resistivity of the plasma is everywhere enhanced from zero to some finite value, beginning at $t=0$. This leads to simple, resistive diffusion of the current sheet, which then couples to the global field via FMS waves.

The enhanced-resistivity model for transient reconnection is adopted for simplicity, and to make contact with previous investigations. Forbes *et al.*¹⁸ studied the effect of sud-

denly enhanced resistivity on an infinite current sheet. They found that the diffusion coupled to outgoing FMS waves. Unfortunately, the diffusion could not decrease the current due (as alluded to above) to the uniform external field. Studies of infinite sheets in two and three dimensions have also adopted a suddenly enhanced resistivity.^{10,19} They found results conforming to the behaviors outlined above.

In this work, we first describe the finite current sheet that forms the initial condition. Then in Sec. III we present the CMH equations. We solve these numerically, using our initial condition, and analyze the behavior of the solution. We find that most of the energy released by reconnection is converted by the outward propagating FMS waves into kinetic energy; a vanishingly small fraction is actually dissipated during the reconnection itself. In Sec. V, we return to consider the limitations of the model itself.

II. RECONNECTION AT A CURRENT SHEET

The prototype of a two-dimensional current sheet, proposed by Green¹⁴ and Syrovatskii,¹⁵ is embedded in an X-point field $\mathbf{B}_0 = -B'(y\hat{x} + x\hat{y})$. The magnetic field is planar and can, in general, be expressed in terms of a flux function, $\mathbf{B} = \nabla A \times \hat{z}$. The current sheet field uses a flux function written as the real part of a complex function, $A(x, y) = \text{Re}\{\Psi(x + iy)\}$, where

$$\Psi(w) = \frac{1}{2}B'w\sqrt{w^2 - \Delta^2} - 2I_0 \ln(w + \sqrt{w^2 - \Delta^2}), \quad (1)$$

with constants B' , Δ , and $I_0 = \Delta^2 B'/4$. Due to the Cauchy-Riemann equations, the flux function will be harmonic ($\nabla^2 A = 0$), and thus current-free, wherever $\Psi(x + iy)$ is analytic. This is everywhere except along the branch cut between $x = -\Delta$ and $x = +\Delta$. This singularity is the current sheet across which the magnetic field is discontinuous, as shown in Fig. 1. In spite of this singularity, the magnetic field is a stable equilibrium provided the resistivity is exactly zero.

Away from the current sheet ($r > \Delta$), the flux function can be expanded as a series,

$$A(r, \phi) = \frac{1}{2}B'r^2 \cos(2\phi) - 2I_0 \ln(r/\Delta) + \sum_{m \geq 2} I_0 \frac{j_m}{m} \left(\frac{\Delta}{r}\right)^m \cos(m\phi), \quad (2)$$

with the dimensionless coefficients

$$j_m = \frac{1}{\pi} \int_{-1}^1 u^m \sqrt{1 - u^2} du = \frac{1 \cdot 3 \cdots (m-1)}{2 \cdot 4 \cdots m \cdot (m+2)}$$

for even integers m . The first term on the right-hand side of Eq. (2) produces the simple X-point $\mathbf{B}_0(x, y) = -B'(y\hat{x} + x\hat{y})$. The remaining terms result from the current, I_0 , distributed within the sheet, and can be considered a perturbation to the X-point field. Reconnection occurring within that sheet will diminish or completely eliminate the current, thereby changing those terms in the flux function. We will explore the dynamics whereby this local change propagates to the far field.

The most significant changes in the far field will be in the $m=0$, logarithmic term, second on the right of Eq. (2).

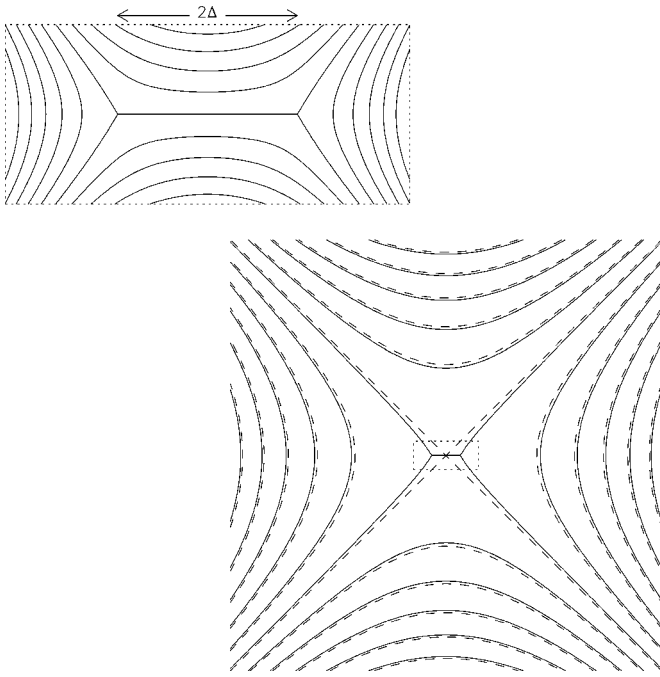


FIG. 1. The magnetic field of an equilibrium current sheet. Solid lines are contours of $A(x,y)$, which trace field lines. Dashed lines show the contours of A_0 , which are field lines of the unperturbed X-point field. The inset, surrounded by dotted lines, is a close-up of the neighborhood of the current sheet.

That term alone is related to the value of A on the separatrix. Changes in this value are a manifestation of reconnection flux transport, so $m=0$ perturbations alone are termed “topological perturbations.”¹⁶

Furthermore, the $m=0$ term contains virtually all of the magnetic energy in the perturbation. The magnetic energy integral

$$W_m = \frac{1}{8\pi} \int |\nabla A|^2 r dr d\phi \quad (3)$$

of the full flux function converges in any finite region including the sheet. When extended to large radius L , the $m=0$ contribution to the integral is

$$I_0^2 \int_r^L \frac{dr}{r} \sim I_0^2 \ln(L),$$

which diverges as $L \rightarrow \infty$; all other perturbation contributions converge. The small current sheet thereby contains a significant amount of energy distributed throughout the magnetized volume. This energy, almost entirely in the $m=0$ mode, will be released by the elimination of the current sheet.

III. DYNAMICS OF THE AXISYMMETRIC MODE

A. The model equations

We study the dynamical evolution of the magnetic field as a result of the dissipation or reconnection of the current sheet above. The dissipation is accomplished by introducing a uniform resistivity η at $t=0$. We demonstrate below that there is a natural dissipation length scale $\ell_\eta \sim \eta^{1/2}$. In order to simplify our analysis, we assume η to be large enough that

$\ell_\eta \gg \Delta$ the size of the sheet. As a result of this assumption, the dynamics can be approximated by linearizing the resistive magnetohydrodynamics (MHD) equations about the X-point equilibrium $\mathbf{B}_0 = \nabla A_0 \times \hat{\mathbf{z}}$,

$$\frac{\partial \mathbf{B}_1}{\partial t} = -\nabla(\mathbf{v}_1 \cdot \nabla A_0) \times \hat{\mathbf{z}} + \eta \nabla(\nabla^2 A_1) \times \hat{\mathbf{z}}, \quad (4)$$

$$\frac{\partial \mathbf{v}_1}{\partial t} = -\frac{\nabla A_0}{4\pi\rho_0} \nabla^2 A_1, \quad (5)$$

where the subscript 1 designates perturbations. Following CMH,^{16,17} the plasma pressure is neglected for simplicity.

A defining feature of the X-point field (the unperturbed field) is that its magnitude increases linearly with radius, as $|\mathbf{B}_0| = B' r$. The Alfvén speed of the field, therefore, increases similarly: $v_{A,0} = \omega_A r$, where $\omega_A = B' / \sqrt{4\pi\rho_0}$ is a characteristic frequency. The corresponding time scale, $1/\omega_A$, is the time taken for an Alfvénic disturbance to travel inward from a radius r to a radius r/e . The diffusivity and Alfvén frequency together define the diffusive radius

$$\ell_\eta = \sqrt{\eta/\omega_A}. \quad (6)$$

In order to consolidate the notation, we introduce the variables

$$C(r,t) = rB_\phi = -r \frac{\partial A_1}{\partial r}, \quad (7)$$

$$U(r,t) = \mathbf{v}_1 \cdot \nabla A_0 = -\hat{\mathbf{z}} \cdot (\mathbf{v}_1 \times \mathbf{B}_0), \quad (8)$$

related to the enclosed current and the motional electric field, respectively. Both C and U are assumed independent of ϕ in order to focus on the dynamics of the $m=0$ mode. The $m=0$ component of C is related to the net current inside a radius r ,

$$I_{\text{enc}}(r) = \frac{1}{4\pi} \oint \mathbf{B}_1 \cdot d\mathbf{l} = \frac{1}{2} r B_\phi = \frac{1}{2} C(r). \quad (9)$$

Note that an axisymmetric $U(r,t)$ corresponds to a velocity field with ϕ dependence akin to $m=2$. Where $U > 0$, there is outward flow along the x axis and an inward flow along the y axis.

Equations (4) and (5) can be used to form a pair of coupled linear PDEs for the $m=0$ components of C and U ,

$$\frac{\partial C}{\partial t} = r \frac{\partial U}{\partial r} + \eta r \frac{\partial}{\partial r} \left(\frac{1}{r} \frac{\partial C}{\partial r} \right), \quad (10)$$

$$\frac{\partial U}{\partial t} = \omega_A^2 r \frac{\partial C}{\partial r}. \quad (11)$$

These two can be combined into the single higher-order equation

$$\frac{\partial^2 C}{\partial t^2} = \omega_A^2 r \frac{\partial}{\partial r} \left(r \frac{\partial C}{\partial r} \right) + \eta r \frac{\partial}{\partial r} \left(\frac{1}{r} \frac{\partial^2 C}{\partial t \partial r} \right), \quad (12)$$

closer to the one actually studied by Craig and McClymont¹⁶ and by Hassam.¹⁷ They solved a version of this equation for the flux function, A_1 , inside a finite cylinder, $r \leq L$. Hassam

found closed-form expressions, in terms of hypergeometric functions, for damped-harmonic eigenmodes satisfying the condition $A_1(L, t) = 0$.

At large distances, $r \gg \ell_\eta$, the dissipative term (second on the right) may be dropped from Eq. (10). What remains is a pair of telegraphers equations in the coordinate $R = \ln r$. Solutions to these can be written in terms of a single arbitrary function, $F(x)$, of one variable,

$$C(r, t) = C_0 - F(\omega_A t \mp \ln r), \quad (13)$$

$$U(r, t) = \pm \omega_A F(\omega_A t \mp \ln r), \quad (14)$$

where C_0 is a constant. The upper or lower signs correspond to an FMS disturbance propagating outward or inward, respectively. The arbitrary function F describes the structure of the disturbance that propagates without dispersion at the radially increasing Alfvén speed; this is also the FMS speed since the sound speed vanishes in our approximation.

Inward disturbances decelerate exponentially as they approach the origin. CMH^{16,17} studied the evolution of disturbances propagating inward from an outer boundary $r=L$, and thus took $C_0=0$. After a time $\sim \omega_A^{-1} \ln(L/\ell_\eta) \sim -\ln \eta$, the waves reached a radius where the dissipative term could no longer be ignored. They were reflected and partially absorbed there.

We are interested instead in solutions that are initiated from the center and propagate only outward. We take the system to be initially stationary, so $U(r, 0) = 0$ and the function $F(x) \rightarrow 0$ as $x \rightarrow -\infty$. We also assume that the magnetic field is initially given by the $m=0$ component of the field outside a current sheet, as given by expression (2). Noting that $C = -r(\partial A / \partial r)$, we find that the current sheet sets the constant $C_0 = 2I_0$. The outward propagating disturbance will take the form of a positive F representing the diminished current left behind by the reconnection.

Immediately after the resistivity is initiated ($t=0$), there will be little motion and the first term on the right-hand side of Eq. (10) may be neglected. What remains is a kind of diffusion equation for $C(r, t)$. The rationalized current density, $J = r^{-1}(\partial C / \partial r)$, satisfies the traditional diffusion equation,

$$\frac{\partial J}{\partial t} = \eta \frac{1}{r} \frac{\partial}{\partial r} \left(r \frac{\partial J}{\partial r} \right) = \eta \nabla^2 J. \quad (15)$$

A simple solution to this beginning as the current of an infinitesimally thin wire, $J(\mathbf{x}, t) \propto \delta(\mathbf{x})$, is

$$J_d(r, t) = \frac{C_0}{2\eta t} \exp\left(-\frac{r^2}{4\eta t}\right). \quad (16)$$

The actual initial condition for the diffusive phase will reflect the internal structure of the current sheet of breadth 2Δ . In the limit $\Delta/\ell_\eta \rightarrow 0$, the structure will diffuse away rapidly leaving a current density similar to expression (16). We will hereafter use this as the initial condition. Since ℓ_η is the only length scale in the problem, we may use it as the unit of length, without loss of generality, and the solution will apply to an arbitrary diffusivity $\eta \neq 0$.

The other functions corresponding to Eq. (16) are

$$C_d(r, t) = C_0 - C_0 \exp\left(-\frac{r^2}{4\eta t}\right), \quad (17)$$

$$U_d(r, t) = \frac{C_0 \omega_A^2 r^2}{2\eta} E_1\left(-\frac{r^2}{4\eta t}\right), \quad (18)$$

where E_1 is the exponential integral. The diffusive solution applies only to early times, just after the enhancement of the resistivity.

B. The solution

Equations (10) and (11) are solved numerically using expressions (17) and (18) as initial conditions. The equations are reformulated in terms of the logarithmic variable $R = \ln(r/\ell_\eta)$, for which $r(\partial/\partial r) = \partial/\partial R$ is a simple derivative.^{16,17} (Since we use ℓ_η as the unit, this logarithmic variable is also written simply as $\ln r$). The two functions are represented on uniform staggered grids in R . The two equations are advanced alternately and the diffusive term is advanced implicitly in an operator splitting method. The solution is begun with expressions (17) and (18) at some time safely within the diffusive regime: Typically $t = 0.001/\omega_A$. The grid extends from $R = -7$ to 20, which is more than 11 orders of magnitude in radius ($r = \ell_\eta e^{-7}$ to $r = L = \ell_\eta e^{20}$) but does not include the origin. At the left edge ($R = -7$), velocity and current are set to zero. At the right edge, $R = 20$, $U = 0$, and $\partial C / \partial R = 0$, but the run is stopped before the disturbance reaches this boundary.

Figure 2(a) shows the solution $C(r)$ at successive times. The diffusive solution, C_d (dashed), is a good approximation until $t \approx 0.5/\omega_A$. After that time, the right portion of the curve begins to resemble the outward-propagating wave solution of Eq. (13). The transition from diffusive to propagating behavior is clearly seen in Fig. 2(b) showing the location where $C(r, t) = \frac{2}{3}C_0$ as a function of time.

The emerging wave nature of the solution is evident in Fig. 3, which shows both $C(r, t)$ and $U(r, t)$. Outside of the diffusion region, $\ln r > 0$, the velocity variable $U(r, t)$ begins to grow and resemble a rightward moving pulse complementary to $C(r, t)$. The sum $C + U/\omega_A$ (not shown) is almost exactly flat over the region $\ln r > 0$. Uniformity of this sum is a property of an outward propagating solution (upper sign) in Eqs. (13) and (14).

The basic behavior evident in the solution is that the current formerly concentrated at the X-point has diffused outward and then propagated away as a FMS pulse. The pulse contains a significant fraction of the initial current in a narrow, but not infinitesimal, sheath. The shape of C is not dispersed in the variable $\ln r$, so the width of the actual sheath is proportional to radius.

In its wake, the pulse leaves a flow whose sense, $U > 0$, is that required for reconnection at a horizontal current sheet: Inward along the y axis and outward along the x axis. The flow is relatively steady in spite of the transient nature of the wave that established it. In addition to the rightward propagation of the wave, the flow field encroaches slowly toward the origin (leftward). We show below that this is the result of advection from the wave interacting with diffusion.

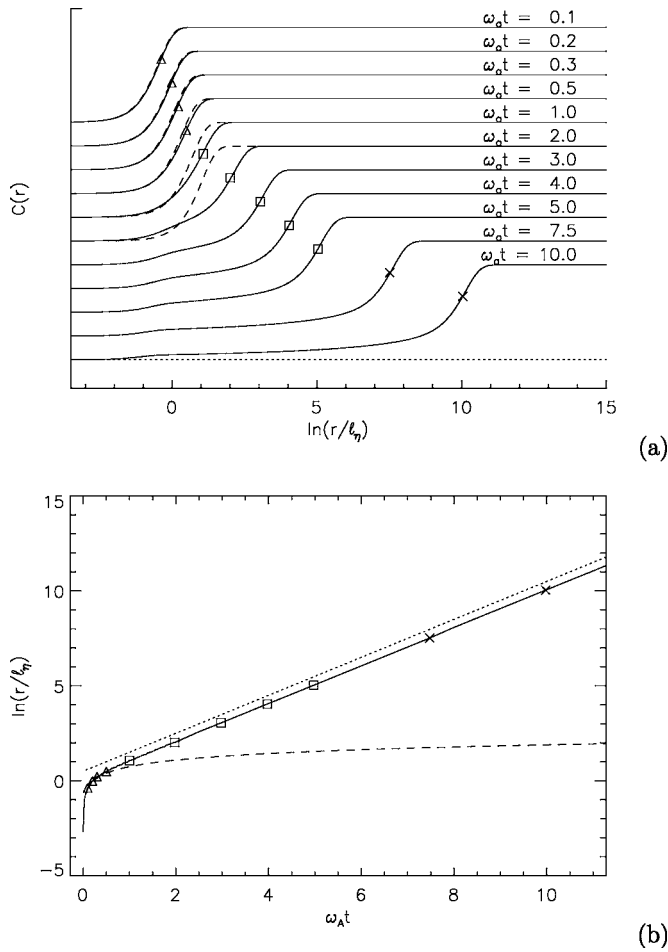


FIG. 2. The solution of the current $C(r,t)$. (a) Plots of the solution at successive times displaced vertically for clarity. These are at times $\omega_A t = 0.1, 0.2, 0.3, 0.5, 1, 2, 3, 4, 5, 7.5,$ and 10 from top to bottom. For each curve, the left side is at $C=0$ and the right is at $C=C_0$, and a symbol marks $C = \frac{2}{3}C_0$. Dashed curves show the diffusive solution, $C_d(r,t)$, for the first several times. (b) The location $C = \frac{2}{3}C_0$ as a function of time (solid). Symbols correspond to the times from (a). The dashed curve is the diffusive motion: $r_d = \sqrt{4\eta t \ln 3}$. Dotted line is the wave motion, $r_w = \ell_\eta e^{\omega_A t}$.

C. The reconnection rate

The outward propagating pulse sets up an approximately steady reconnection flow, whose effect at the X-point is illustrated by the flux function. We calculate A from the numerical solution

$$A(r,t) = \int_r^L C(r',t) \frac{dr'}{r'}, \tag{19}$$

where $L = \ell_\eta e^{20}$ is the outer (right) boundary. Figure 4 shows these curves at successive times (right) as well as its value at the left of the grid, used as a proxy for the X-point: $\approx A(0,t)$.

During the initial phase, $t < 0.5/\omega_A$, the curve follows the purely diffusive behavior

$$A(0,t) \approx A(0,t_0) - \frac{1}{2}C_0 \ln(t/t_0), \tag{20}$$

predicted from the Ohmic electric field at the X-point: $\partial A/\partial t = -\eta J$, with J from Eq. (16).

The electric field is, however, determined by the wave solution. The magnetosonic pulse is approximately a sheath

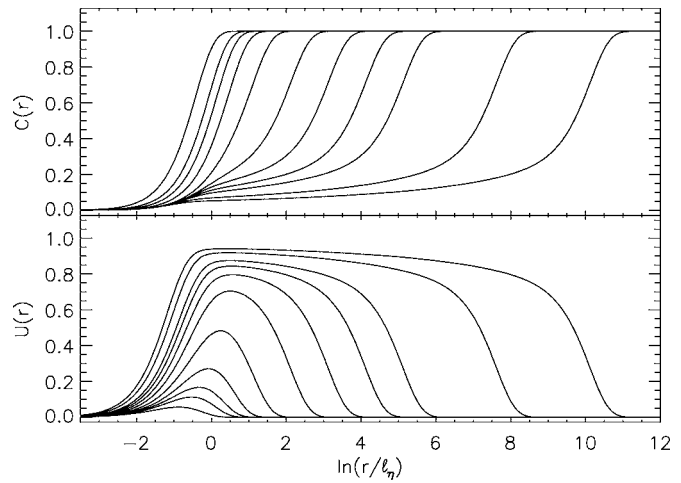


FIG. 3. Plots of the functions $C(r,t)$ (top) and $U(r,t)$ at the same times as in Fig. 2. Successive times are plotted on the same axis, but generally run from left to right.

of current at a radius s moving outward ($\sim e^{\omega_A t}$). This sheath possesses a current $C(r) = C_0 \Theta(r-s)$, where Θ is the Heaviside function. It thus creates a flux function $A = C_0 \ln(L/s)$ inside the sheath ($r < s$) according to Eq. (19). The result is that the flux function is relatively flat inside the sheath with a level that decreases linearly with time, as seen in Fig. 4.

This latter behavior, driven by the outer wave solution, would seem to be inconsistent with the diffusive solution near the origin. The secular decrease mandated by the wave requires a persistent, roughly constant electric field, $E = -\partial A/\partial t$, at the X-point. This is at odds with the decreasing electric field of the diffusive inner solution.

The resolution of the paradox comes from a third regime, suggested in a plot of the current density, $J(r,t) = r^{-1} \partial C/\partial r$, shown in Fig. 5. The current density initially tracks the diffusive behavior of Eq. (16), broadening over

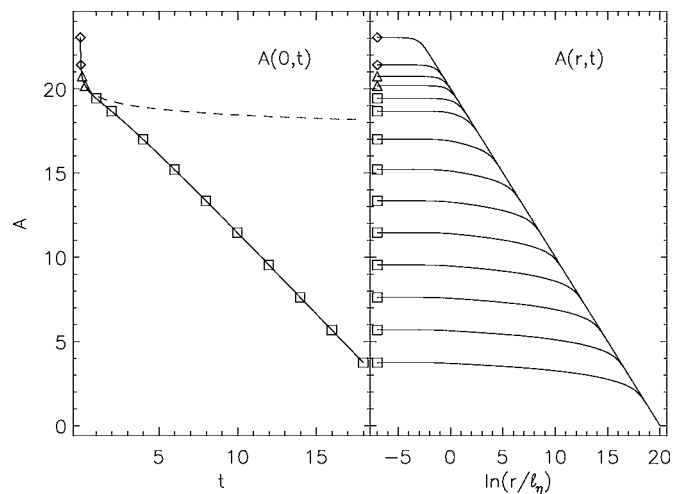


FIG. 4. Plots of the flux function $A(r,t)$ calculated from the numerical solution. (Right) Plots of $A(r)$ at times, $\omega_A t = 0.01, 0.03, 0.1, 0.3, 1, 2, 4, 6, \dots$ reading from top to bottom. (Left) The value of A at the left grid point vs time (in units of $1/\omega_A$). Symbols on the curve correspond to the curves from the right panel. The dashed curve shows the purely diffusive behavior of Eq. (20).

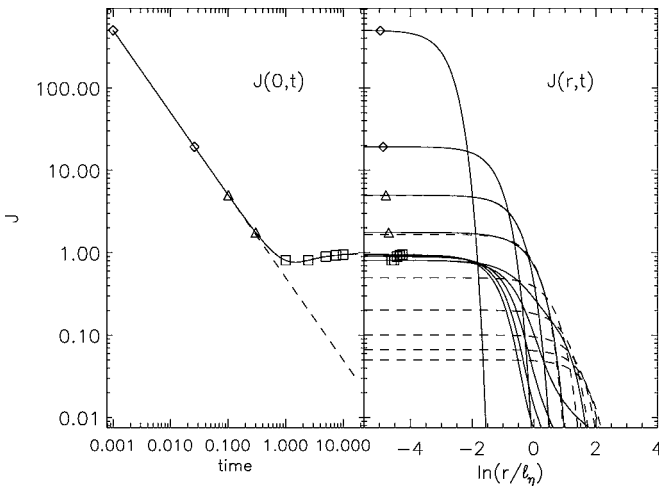


FIG. 5. Plots of the current density, J , at the same times shown in Fig. 4. (Right) The profiles at successive times. Dashed lines show the diffusive solution, Eq. (16). (Left) The current density on axis, $J(0,t)$, plotted vs time on a logarithmic scale. The diffusive solution is plotted with a dashed line.

time and diminishing in amplitude to preserve total current. The peak amplitude (left) initially decreases [$J(0,t) \sim 1/t$], following the dashed line. At $t \approx 0.5/\omega_A$, however, this behavior ceases and the peak remains at $J(0,t) \approx C_0/\ell_\eta^2$. At the same time, the profile (right) stops spreading outward and actually begins to contract toward the origin.

This new regime in the solution is characterized by a balance between diffusion and wave advection, which occurs near the X-point at times $t > 0.5/\omega_A$. Under this balance, the term on the left-hand side of Eq. (10) is negligible, leaving

$$0 = r \frac{\partial}{\partial r} (U + \eta J). \quad (21)$$

The solution to this consistent with $U(0,t) = 0$ is

$$U(r,t) = \eta [J(0,t) - J(r,t)]. \quad (22)$$

Placing this into Eq. (11) leads to a differential equation for $J(r,t)$ in the vicinity of the X-point,

$$\frac{\partial J}{\partial t} + \frac{\omega_A^2 r^2}{\eta} J = J_t(0,t), \quad (23)$$

where the subscript here denotes partial differentiation. This is an ordinary differential equation at each radius, whose general solution, beginning at some time t_0 , is

$$J(r,t) = J(r,t_0) e^{-\omega_A^2 r^2 (t-t_0)/\eta} + \int_{t_0}^t J_t(0,t') e^{-\omega_A^2 r^2 (t-t')/\eta} dt'. \quad (24)$$

It is evident from the numerical solution that after time $t = t_0 = 0.5/\omega_A$ the current at the X-point remains roughly constant. This means that $J_t(0,t) \approx 0$ for $t \geq t_0$, and the second term on the right of Eq. (24) can be dropped. We may furthermore use the purely diffusive solution, Eq. (16), for $J(r,t_0)$, to get

$$J_{ald}(r,t) = \frac{C_0 \omega_A}{\eta} \exp\left(-\frac{\omega_A^2 r^2 t}{\eta}\right), \quad (25)$$

for $t > 0.5/\omega_A$. We refer to this as the *advective/diffusive* solution. The remaining functions corresponding to it are

$$C_{ald}(r,t) = \frac{C_0}{2\omega_A t} \left[1 - \exp\left(-\frac{\omega_A^2 r^2 t}{\eta}\right) \right], \quad (26)$$

$$U_{ald}(r,t) = C_0 \omega_A \left[1 - \exp\left(-\frac{\omega_A^2 r^2 t}{\eta}\right) \right]. \quad (27)$$

The solutions from the new regime, Eqs. (25)–(27), explain the behavior observed in Figs. 4 and 5. The current density remains roughly constant, $J_{ald}(0,t) = C_0/\ell_\eta^2$, but is restricted to a shrinking region,

$$r < r_{ald} = \frac{\ell_\eta}{\sqrt{\omega_A t}}. \quad (28)$$

The electric field on the axis, $\eta J_{ald}(0) \sim C_0 \omega_A$, remains constant, causing the secular decrease in the flux function after $t \approx 0.5/\omega_A$. Since the persistent electric field is independent of η , the regime represents truly fast reconnection. In retrospect, this is inevitable since the internal solution must match an external solution in which η plays no role.

The flow field U_{ald} , in Eq. (27), has a fixed maximum, but encroaches inward as $r_{ald} \sim t^{-1/2}$. This progression was noted in Fig. 3. While the same regime was studied by Hassam,¹⁷ his solution began at the exterior and was therefore never able to create current at the X-point. Consequently, he observed the regime as a slow (nonexponential) decay in current there, rather than a persistent current.

D. Approximate analytical solution

It is possible to approximate the complete solution analytically by combining the elements of analysis presented above. Prior to $t = 0.5/\omega_A$, the entire solution behaves diffusively and is well described by Eqs. (16)–(18). After that time, the internal solution, for $r < r_0$, some fixed radius, will follow Eqs. (25)–(27). The solution external to this will be a traveling solution, like Eqs. (13) and (14), whose function $F(x)$ is set to match the inner one. In particular,

$$C(r_0,t) = C_0 - F(\omega_A t - \ln r_0) = C_{ald}(r_0,t). \quad (29)$$

Setting this equal to Eq. (26) gives a function

$$F(x) = C_0 - \frac{C_0}{2(x + \ln r_0)} \left\{ 1 - \exp\left[-\frac{\omega_A(x + \ln r_0)r_0^2}{\eta}\right] \right\}.$$

Using this in the solutions yields the outer analytic solutions

$$C_a(r,t) = \frac{C_0}{2(\omega_A t - \ln r/r_0)} \times \left\{ 1 - \exp\left[-\frac{(\omega_A t - \ln r/r_0)r_0^2}{\eta}\right] \right\}, \quad (30)$$

which applies to $r < r_0 e^{\omega_A t}$. Beyond that radius $C = C_0$ since the disturbance has not yet reached it.

Figure 6 shows the numerical solutions from Fig. 2, along with the analytic approximation C_a (dashed), using

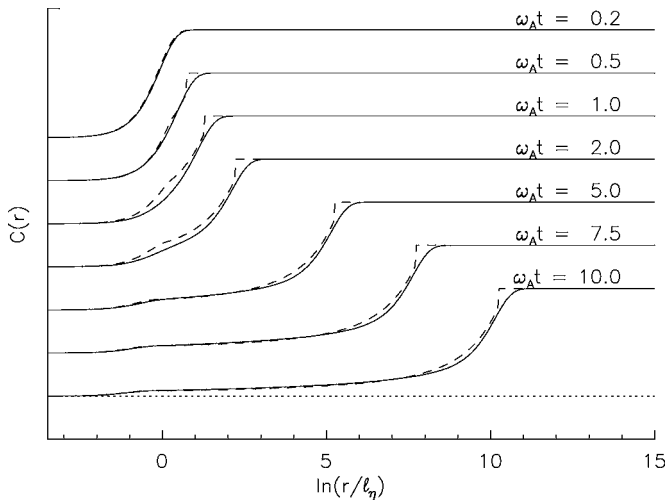


FIG. 6. The numerical solution $C(r, t)$ at various times, as in Fig. 2. Here the analytic approximation, $C_a(r, t)$, from either Eq. (17), Eq. (26), or Eq. (30), is shown as dashed curves.

$r_0 = 0.25\ell_\eta$. The fit is reasonably good for all the times. Times near $t = 1/\omega_A$ represent the merging of the two regimes and thus are fit the worst.

Diffusive effects become increasingly irrelevant as the pulse moves outward. Thus we expect the true solution to follow this behavior even beyond the extent of our numerical grid. Furthermore, the advective/diffusive solution, given by Eqs. (25)–(27), appears increasingly accurate at later times. We therefore have a good approximation to the complete solution valid at least until the assumption of linearity fails (to which we return below).

IV. ENERGETIC CONSEQUENCES

The magnetic and kinetic energy of the $m=0$ perturbations, between radii a and b , are

$$W_m = \frac{1}{4} \int_a^b C^2 \frac{dr}{r}, \tag{31}$$

$$W_k = \frac{1}{4} \omega_A^{-2} \int_a^b U^2 \frac{dr}{r}. \tag{32}$$

The time derivative of the sum of these energies can be re-written in the form

$$\frac{d}{dt}(W_m + W_k) = \frac{1}{2} C(U + \eta J) \Big|_a^b - \frac{1}{2} \eta \int_a^b J^2 r dr. \tag{33}$$

The first term on the right of Eq. (33) represents Poynting flux into or out of the annular region. The second term, which is never positive, is the Ohmic heating loss.

Figure 7 shows the profiles of both the Poynting flux, $C(U + \eta J)$, and the logarithmic density of Ohmic dissipation, $\eta r^2 J^2$, computed from the numerical solution. The Ohmic dissipation is plotted on a logarithmic scale since it drops dramatically after $t = 1/\omega_A$. The roughly constant current carried outward by the magnetosonic pulse is distributed over a homologously expanding sheath causing $J \sim r^{-2}$. The dashed

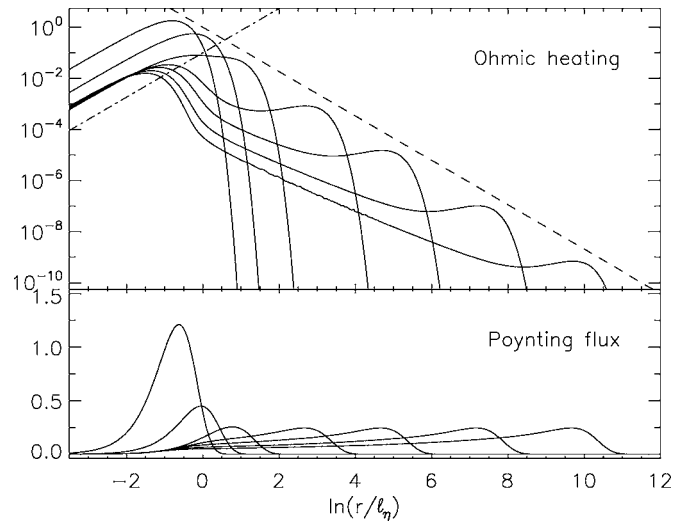


FIG. 7. Plots of the contributions to the changes in total energy at successive times. Times $\omega_A t = 0.1, 0.3, 1, 3, 5, 7.5, 10$ are plotted on a common axis, progressing from left to right. (Top) The density in R of the Ohmic loss term: $\eta r^2 J^2$ on a logarithmic scale. The dashed and broken curves show r^{-2} and r^2 for reference. (Bottom) The Poynting flux $C(U + \eta J)$.

line in Fig. 7 confirms this tendency showing that $\eta r^2 J^2 \sim r^{-2}$. Meanwhile the inner advective/diffusive solution, characterized by $J \sim C_0/\ell_\eta^2$, contributes a factor $\sim r^2$ to the heating density (broken line). As a result, there is very little Ohmic dissipation after the diffusive phase ends.

The Poynting flux, plotted on the bottom of Fig. 7, shows a shifting of energy first inward, then outward. In the wave-dominated region it becomes a simple positive pulse traveling outward without diminishing. A particular annulus at $r \gg \ell_\eta$ will first experience an energy decrease as this pulse crosses its inner boundary [only the lower limit in Eq. (33) will contribute]. This inward flux is natural since the initial diffusion left a deficit of magnetic pressure at the X-point. After its leading edge passes the outer radius, the pulse’s negative slope will produce an energy increase within the annulus [the upper limit exceeding the lower limit in Eq. (33)]. In the end, the Poynting flux term goes back to zero, so it will not have changed the net energy in that annulus.

While the magnetosonic pulse does not increase or decrease net energy, it does produce a significant energetic effect. Figure 3 clearly shows that C is decreased and U is increased in the wake of the leading edge. According to Eqs. (31) and (32), this reflects a conversion of magnetic to kinetic energy. A plot of the total kinetic energy within the numerical grid (Fig. 8) confirms this. The kinetic energy increases linearly in time once the wave nature of the solution has become established ($t > 1/\omega_A$). This is another manifestation of the persistent reconnection flow left in the wake of the moving current sheath.

It is noteworthy that the Ohmic heating is a minor factor in the energy budget after the dissipative phase. Our solution began as an infinitely thin wire, whose initial diffusion liberates an infinite amount of energy. To accommodate this artificial initial state, Fig. 8 plots the integral of Ohmic dissipation forward from $t = 1/\omega_A$. The curve therefore diverges, logarithmically, in the negative sense as $t \rightarrow 0$. Had we used

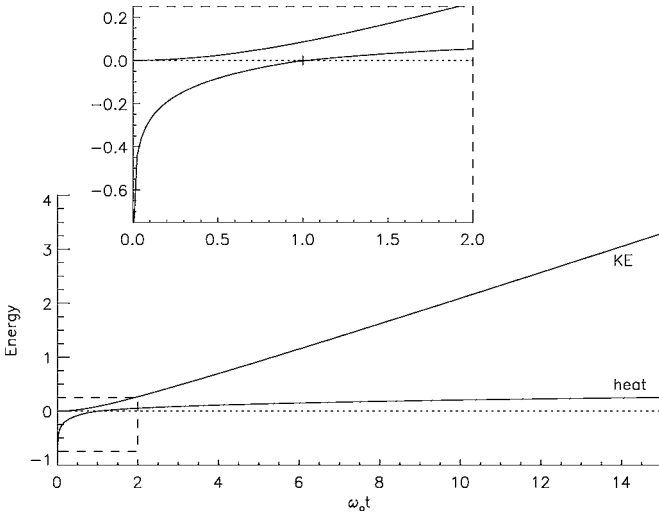


FIG. 8. The kinetic energy and integrated heating loss plotted vs time. The inset is an expansion of the early phase, which includes the diffusive regime. The heating loss is integrated from $t=1/\omega_A$, and is therefore negative for $t < 1/\omega_A$.

the actual current sheet as an initial condition, there would be no divergence, in spite of the singular current density. The Ohmic dissipation cannot release more than the finite magnetic energy density in the neighborhood of the current sheet: $\sim \ln(\ell_\eta/\Delta)$. This entire conversion would occur in about the same time indicated by Fig. 8: $\sim 1/\omega_A$.

After the initial diffusive phase, the magnetic energy is converted almost entirely to kinetic energy. This occurs in spite of the persistent electric field at the X-point. That electric field continues to transfer magnetic flux at the Alfvénic rate, but does so with very little energy dissipation. While the current density at the X-point remains fixed, it is confined to a shrinking region, and therefore accounts for an ever decreasing net current $I=2C(0) \sim 1/t$. The net electrodynamic work done by the electric field, therefore, becomes logarithmic, as the figure shows.

The persistent X-point current stores a residual magnetic energy. The magnetic energy inside the diffusion radius,

$$W_x \sim I^2(t) \ln(\ell_\eta/r_{ad}) \sim \frac{\ln(\omega_A t)}{t^2}, \quad (34)$$

diminishes rapidly due to the diminishing current, in spite of its concentration toward the origin. The Ohmic dissipation power, $P_\eta = EI \sim 1/t$, small as it is, cannot be supplied by this residual magnetic energy. Instead the dissipated energy must be supplied by the encroaching flow.

Meanwhile, the outward propagating magnetosonic pulse continues to transform magnetic energy in the far field into kinetic energy. We began our discussion by noting the extensive (potentially infinite) magnetic energy available in the $m=0$ component of the magnetic perturbation. Adding the two curves in Fig. 8 to the total magnetic energy within the numerical solution does yield a constant value. The system conserves total energy, at least until the solution encounters one of the boundaries.

V. LIMITATIONS OF THE MODEL

A. Breakdown of linearity

The foregoing analysis was performed after dropping from the MHD equations all nonlinear terms. We now check this assumption by estimating the magnitudes of the neglected terms. The ratio of the perturbation field to the equilibrium field will be largest near the X-point, where the equilibrium field vanishes. Using the diffusive solution, Eq. (17), in the vicinity of the origin gives a ratio

$$\frac{|\mathbf{B}_1|}{|\mathbf{B}_0|} \sim \frac{C(r)}{r^2 \omega_A^2 \sqrt{4\pi\rho_0}} \approx \frac{\epsilon}{2\omega_A t}, \quad (35)$$

where we have introduced the dimensionless amplitude

$$\epsilon = \frac{I_0}{\eta \sqrt{4\pi\rho_0}} = \frac{1}{4} \frac{\Delta^2}{\ell_\eta^2}. \quad (36)$$

The denominator in the second expression of Eq. (36) is a current, $I_{sp} = \eta \sqrt{4\pi\rho_0}$, characteristic of the diffusive plasma. The Lundquist number at the original current sheet is²⁰ $S_\Delta = \sqrt{I_0}/I_{sp}$. The current sheet, and thus the perturbation, is generally small if it carries a net current much less than I_{sp} . A restatement is that the resistive enhancement must increase I_{sp} to a level much larger than the current in the sheet. This also means, not coincidentally, that the initial sheet underwent diffusion at a very small Lundquist number $S_\Delta = \epsilon^{1/2} \ll 1$.

Even if $\epsilon \ll 1$, it would appear at first sight, from Eq. (35), that the linear approximation fails during early times, $\omega_A t \ll \epsilon$. Indeed, a current sheet creates a finite magnetic field that cannot be considered as a small perturbation to the vanishing magnetic field of the X-point; a wire creates an infinite field, making matters still worse. During the early times being considered, however, the evolution is dominated by diffusion, which involves two inherently linear terms. In that case, the appropriate comparison is between the neglected nonlinear term and the diffusive one. This is equivalent to the ratio of electric fields,

$$\frac{|\mathbf{v}_1 \times \mathbf{B}_1|}{\eta J_d} \sim \frac{|\mathbf{B}_1|}{|\mathbf{B}_0|} \frac{U_d}{\eta J_d} \sim \epsilon \left(\frac{r}{\ell_\eta} \right)^2 E_1 \left(\frac{-r^2}{4\eta t} \right) e^{r^2/4\eta t},$$

which is $\sim \epsilon$ even as $r \rightarrow 0$ or as $t \rightarrow 0$. Thus the diffusion of the intense currents overwhelms any potential nonlinear effects, at least in the early stages.

At later times, the solution enters its advective/diffusive regime for which $|\mathbf{B}_1|/|\mathbf{B}_0| \sim \epsilon$. As long as the initial current sheet is small enough, the magnetic field will remain sufficiently small that it will never produce appreciably nonlinear effects.

Nonlinearities might still arise from the velocity, which grows over time. The magnitude of \mathbf{v}_1 can be estimated from U as

$$|\mathbf{v}_1| = \frac{U}{|\mathbf{B}_0|} = \epsilon \frac{U}{C_0 \omega_A r} \approx \epsilon \frac{\eta}{r} \left[1 - \exp\left(-\frac{\omega_A^2 r^2 t}{\eta}\right) \right], \quad (37)$$

after using the advective/diffusive form of U , from Eq. (27). At a given time, t , the maximum velocity

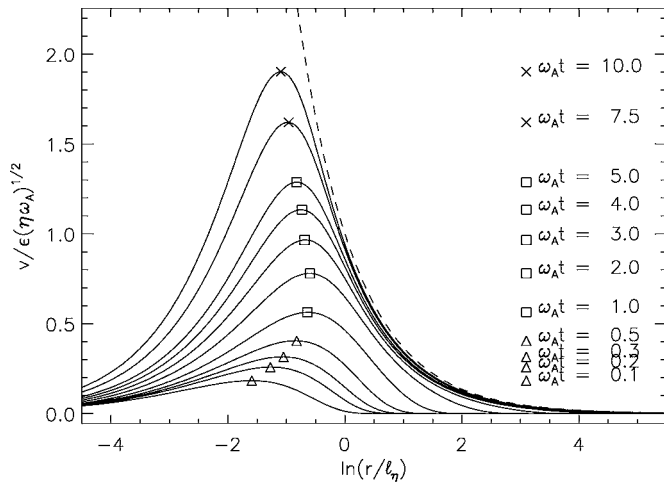


FIG. 9. Plot of the velocity field at the same times as Fig. 2. Peaks are marked and the corresponding times are listed along the right. The dashed line shows the curve $1/r$ for reference.

$$\max|v_1| \approx 0.638\epsilon\ell_\eta\omega_A^{3/2}t^{1/2}$$

occurs at $r_{\max} \approx 1.12r_{al,d}$. This location moves toward the origin, $r_{\max} \sim t^{-1/2}$, even as it grows (see Fig. 9).

As the peak velocity increases ever closer to the X-point, it will eventually exceed the local Alfvén speed of the background field. The ratio of these two,

$$\frac{|v_1|}{v_{A,0}} = \epsilon \frac{U}{C_0} \frac{\eta}{\omega_A^2 r^2} \approx \epsilon\omega_A t, \tag{38}$$

after using the advective/diffusive solution, is obviously an increasing function of time. By the time $\omega_A t \sim \epsilon^{-1}$, the ratio will exceed unity and the linear approximation will have failed. The failure is due to the neglected inertial term becoming comparable to the Lorentz force in the momentum equation.

The continuity equation is not relevant at the linear order due to our assumption that $\beta=0$. Perturbations to density will, however, enter higher-order terms of the momentum equation. The lowest-order source term in the continuity equation, $\rho_0 \nabla \cdot v_1$, will have an $m=2$ azimuthal dependence (i.e., $\sim e^{2i\phi}$), from v_1 . This means that first-order perturbations to density will have $m=2$ and will therefore not directly affect the governing Eq. (11). Any effect from density perturbation will need to enter at still higher order. For example, the second-order perturbation to density is driven by terms such as $\rho_1 \nabla \cdot v_1$, which will affect the $m=0$ governing equations. Such extensive nonlinear analysis is, however, beyond our present scope. We expect that such analysis would reconfirm a breakdown at $t \sim (\epsilon\omega_A)^{-1}$ as already found.

B. Effect from large scales: Reflection

The X-point external field represents the immediate neighborhood of the magnetic neutral point on which the current sheet initially formed (Fig. 10 illustrates this in an example from the solar corona). That field, $B_0 = -B'(y\hat{x} + x\hat{y})$, is the lowest order from an expansion in powers of r . Fast modes propagating away from it will eventually reach

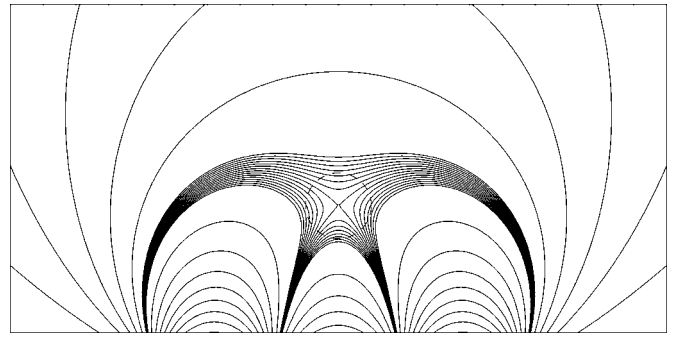


FIG. 10. An illustration of a quadrupolar field in the solar corona containing a null point. The local environment of the null point (dashed circle) resembles the X-point field.

radii where higher orders of the expansion become appreciable. These departures will affect the axisymmetric dynamics near the X-point (i.e., the reconnection) if they lead to reflection of $m=0$ disturbance.

The simplest means of incorporating reflection into the CMH model is by a rigid, conducting boundary at some radius $r=L$ —the approach taken by Craig and McClymont¹⁶ and Hassam.¹⁷ This boundary introduces a second length scale and a characteristic Alfvén speed, $v_{A,0} = \omega_A L$, for which the Lundquist number is $S = \omega_A L^2 / \eta = (L/\ell_\eta)^2$.

The perturbation from reconnection will first reach the boundary at

$$t = \tau_d = \frac{\ln(L/\ell_\eta)}{\omega_A} = \frac{1}{2} \frac{\ln S}{\omega_A}, \tag{39}$$

the same time scale found by CMH. A reflection will then reach the X-point once more at $2\tau_d$, where it will presumably interact with the advective/diffusion solution there.

The rigid, conducting boundary requires conditions $U=0$ and $\partial C/\partial r=0$ at $r=L$ —the same conditions used in our simulation. The second condition is required by the first combined with Eq. (11). In place of the second one, CMH applied the condition $A_1(L)=0$. That condition is not pertinent to our simulation since it is automatically satisfied when A is found from C according to Eq. (19).

To see the nature of reflections due to these conditions, we add to the outward-traveling (upper sign) waves of Eqs. (13) and (14) an inward-traveling wave with undetermined shape function $G(x)$,

$$C(r,t) = C_0 - F(\omega_A t - \ln r) - G[\omega_A t + \ln(r/2L)], \tag{40}$$

$$U(r,t) = \omega_A F(\omega_A t - \ln r) - \omega_A G[\omega_A t + \ln(r/2L)]. \tag{41}$$

The condition $U(L)=0$ is satisfied by setting $G(x)=F(x)$, meaning that the wave reflects without changing shape. Since these functions appear with opposite signs in Eq. (41), the electric field is reversed upon reflection. The choice $G(x)=F(x)$ also satisfies the other boundary condition since

$$\left. \frac{\partial C}{\partial r} \right|_L = \frac{1}{L} F'(\omega_A t - \ln L) - \frac{1}{L} G'(\omega_A t - \ln L) = 0.$$

Well after the incident and reflected waves have both passed a point r , the values there will be $F \approx G \approx C_0$. Using

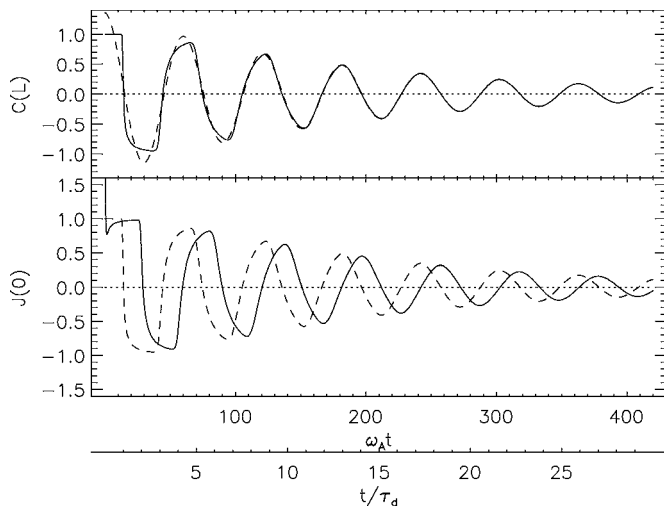


FIG. 11. Plots of the numerical solution inside a rigid, conducting wall at $r=L=\ell_\eta e^{14}$. This radius was chosen to yield a Lundquist number of $S=e^{28}\approx 10^{12}$. Time axes are given in units of $1/\omega_A$ (upper) and $1/\tau_d$ (lower). (Top) The net current enclosed by the outer boundary $C(L)$ (solid). The dashed curve is a fit of the form $\cos(\Omega t)e^{-\gamma t}$, to $t>10\tau_d$. (Bottom) The current density at the origin, $J(0)$ (solid), and a repeat of $C(L)$ (dashed).

this in Eq. (40) yields $C\approx -C_0$, so the current inside r has changed sign. The conducting boundary reflects the current sheath back toward the X-point but with a change of sign.

Figure 11 shows a numerical solution inside a rigid conducting boundary at $L=e^{14}\ell_\eta$. This location makes $S\approx 10^{12}$ roughly characteristic of Spitzer resistivity in the solar corona. Unlike the solution from previous sections, this one continues even after the disturbance reaches that outer boundary. The current, C , enclosed by the outer boundary becomes suddenly negative at $t=14/\omega_A$. This reflected current sheath reaches the diffusive region ($r<\ell_\eta$), reflects *without changing sign*,^{16,17} and reaches the outer boundary once more at $t\approx 42/\omega_A$.

The studies of CMH^{16,17} showed that the diffusive region reflects an incoming pulse with some dispersion and dissipation. Owing to the dispersion, oscillations become more sinusoidal over time. Owing to the dissipation and dispersion, the oscillations decay toward $C=0$. In the end, all of the magnetic energy is converted to heat, provided the X-point is surrounded by a perfectly circular, rigid conducting boundary.

The damped sinusoid in the long-time limit will correspond to the eigenfrequency with the smallest decay rate. Times after $10\tau_d$ [τ_d given by Eq. (39)] fit a damped sinusoid with complex frequency, $\omega\tau_d=1.45-0.080i$ (dashed curve in the upper panel). This is very close to the value at the same Lundquist number, $\omega\tau_d=1.38-0.078i$, found analytically by Hassam.¹⁷

The lower trace in Fig. 11 shows the current density at the X-point. Its initial behavior follows the analysis from the previous sections: Initial decay followed by a return to a constant value during the advective/diffusive phase. The arrival of the reflected pulse at $t=28/\omega_A$ injects opposing current into the X-point. This overwhelms the small peak remaining from the initial current sheet, driving $J(0)$ negative. Indeed, each subsequent reflection changes its sign once

more and $J(0)$ undergoes damped oscillations that lag those of $C(L)$ by 90° . One complete cycle requires two complete reflections and therefore takes $4\tau_d$.

The initial reflection will reverse the process of energy conversion. On the outside of the reflected sheath, $C=-C_0$ and $U=0$, so there is magnetic energy and little kinetic energy. This restored situation will persist until the sheath reflects once more from the X-point and magnetic energy is once again converted to kinetic energy. The rigid conductor creates a cavity oscillator with damping from dissipation at the X-point. This was the finding of the CMH studies.

A perfectly circular boundary is an artificial representation of the effects reflections might have in a realistic situation, such as Fig. 10. A boundary that is not perfectly circular will tend to reflect and “scatter” the disturbance into other azimuthal modes $m\neq 0$. The $m=0$ component of the reflection will thus be much smaller and will not completely reverse the effects of the outgoing wave. The flow established in the wake of the outgoing wave would not be canceled by an equal and opposite reflection. Instead, reflected waves with other spatial structure would interact with the outgoing wave in complex patterns. The resulting dynamics could probably be described as phase mixing as the many eigenmodes initiated by the initial disturbance became dephased with one another. Those with $m\neq 0$ have little amplitude near the X-point and hence would be only weakly damped. The main mechanism for damping would probably resemble the phase-mixing mechanism studied by Heyvaerts and Priest²¹ and others.^{22,23} If this were the case, the energy liberated by the reconnection would be dissipated over a volume much larger than the X-point.

Using the same reasoning, waves reflected by a noncircular boundary will not converge uniformly on the X-point. The result would perhaps resemble studies by McLaughlin and Hood^{24,25} of a multimode disturbance interacting with an X-point. It is not clear how much of the advective/diffusive solution at the X-point would be affected by this kind of reflection.

VI. DISCUSSION

One of the most challenging aspects of magnetic reconnection is that microscopic processes, such as diffusion, couple to global scales. The foregoing model, while highly idealized, provides a tractable illustration of this coupling between the fundamental processes of diffusion and wave propagation (normally studied separately). Diffusion disrupts the current sheet and drives current to a radius where magnetic forces can take effect. These forces create an inflow and outflow pattern that propagates away from the X-point as a FMS wave.

The magnetosonic wave launched by the X-point reconnection communicates changes in the sheet’s current to the global field. The $m=0$ component of the wave, considered here, is a concentric sheath of current approximately matching the net current in the sheet. The field inside this sheath is therefore much closer to potential, so magnetic energy has been lowered.

The magnetosonic wave propagates at the Alfvén speed independent of the resistivity. In order to accommodate these fast dynamics, it is necessary to transfer flux across the X-point at a rate also independent of resistivity. This is accomplished by a current density peak of steady amplitude, $J \approx E/\eta$, but diminishing area. This peak is maintained against diffusion by a flow field encroaching toward the X-point. The persistent X-point electric field continues flux transfer but accomplishes little energy dissipation.

We have used an enhanced resistivity as a simple model of transient reconnection. This model can be solved, self-consistently, as a linear system provided the enhanced resistivity is sufficiently large compared to the initial net current in the sheet (i.e., $\epsilon \ll 1$). A more realistic scenario might involve nonlinear, turbulent processes occurring within the current sheet itself. If the turbulence is sufficiently intense, it might have an effect similar to the resistivity of our model, and linear analysis of all three regimes could once more be justified.

For sheets carrying larger initial current, or lower levels of resistivity (i.e., $\epsilon > 1$), the linear approximation would fail. This is the case for current sheets whose Lundquist number, even using enhanced diffusion, is large: $\epsilon \sim S_{\Delta}^2 \gg 1$. Reconnection at such a current sheet will involve complex nonlinear dynamics, such as outflow jets or tearing modes, significantly different from the simple diffusion of our model. The diffusive and advective-diffusive regime from our study will therefore be inapplicable.

Even when the linear approximation does not apply, we expect the response of the far field to resemble that from our model. The complex dynamics at the current sheet will ultimately transfer flux and diminish the current in the sheet, although possibly only by a fraction. Accommodating this relatively sudden change at great distances requires waves propagating outward from the reconnection site, regardless of the reconnection details. By altering the magnetic field far beyond the current sheet itself, these wave-mediated changes remain the primary mode of energy release. They are a consequence of magnetic reconnection, and do not depend on whether the reconnection occurs through resistivity (as we have assumed) or by other possibly more complicated means.

The basic picture emerging from our model is one of a local reconnection process initiating a global process of energy release through magnetosonic waves. The behavior of these waves in a more realistic scenario needs to be studied in a more realistic model. A perfectly concentric rigid boundary probably overestimates the effects of reflection, for reasons we describe above. Moreover, there is a segregation, in two dimensions, of FMS waves from Alfvén waves, which is not as clear in models with more realistic three-dimensional geometry. In such geometries Alfvén modes are likely to be initiated as well, and these are trapped by closed magnetic field lines much more readily than FMS waves. This might

be relevant to recent observations of oscillating loops in the solar corona, apparently triggered by reconnection and/or solar flares.^{26–28}

Extension to more realistic geometry will probably require that a particular plasma regime be specified. The simple X-point considered in our model is common to reconnection in the solar corona, the magnetosphere, and many astrophysical contexts. Reconnection occurs in these plasmas rapidly after some period of slow energy storage. Our model provides an abstract picture of how the localized process of time-dependent magnetic reconnection can initiate the release, by wave-propagation, of magnetic energy stored throughout a large-scale field.

ACKNOWLEDGMENTS

This work was supported by the National Science Foundation.

- ¹J. W. Dungey, *Cosmic Electrodynamics* (Cambridge University Press, Cambridge, 1958).
- ²E. N. Parker, *Astrophys. J.* **128**, 664 (1958).
- ³P. A. Sweet, in *Electromagnetic Phenomena in Cosmical Physics*, edited by B. Lehnert (Cambridge University Press, Cambridge, 1958), p. 123.
- ⁴H. E. Petschek, in *AAS-NASA Symposium on the Physics of Solar Flares*, edited by W. N. Hess (NASA, Washington, D.C., 1964), p. 425.
- ⁵E. R. Priest and T. G. Forbes, *J. Geophys. Res.* **91**, 5579 (1986).
- ⁶V. S. Semenov, M. F. Heyn, and I. V. Kubyshekin, *Sov. Astron.* **27**, 600 (1983).
- ⁷H. K. Biernat, M. F. Heyn, and V. S. Semenov, *J. Geophys. Res.* **92**, 3392 (1987).
- ⁸M. Heyn and V. Semenov, *Phys. Plasmas* **3**, 2725 (1996).
- ⁹V. S. Semenov, N. N. Volkonskaya, and H. K. Biernat, *Phys. Plasmas* **5**, 3242 (1998).
- ¹⁰S. Nitta, S. Tanuma, K. Shibata, and K. Maezawa, *Astrophys. J.* **550**, 1119 (2001).
- ¹¹S. Nitta, S. Tanuma, and K. Maezawa, *Astrophys. J.* **580**, 538 (2002).
- ¹²N. V. Erkaev, V. S. Semenov, and F. Jamitsky, *Phys. Rev. Lett.* **84**, 1455 (2000).
- ¹³S. Chapman and P. C. Kendall, *Proc. R. Soc. London, Ser. A* **271**, 435 (1963).
- ¹⁴R. M. Green, in *Stellar and Solar Magnetic Fields*, Proceedings of the 22nd IAU Symposium, edited by R. Lust (North-Holland, Amsterdam, 1965), p. 398.
- ¹⁵S. I. Syrovatskii, *Sov. Phys. JETP* **33**, 933 (1971).
- ¹⁶I. J. D. Craig and A. N. McClymont, *Astrophys. J. Lett.* **371**, L41 (1991).
- ¹⁷A. B. Hassam, *Astrophys. J.* **399**, 159 (1992).
- ¹⁸T. G. Forbes, E. R. Priest, and A. W. Hood, *J. Plasma Phys.* **27**, 157 (1982).
- ¹⁹M. G. Linton and D. W. Longcope, *Astrophys. J.* **642**, 1177 (2006).
- ²⁰D. W. Longcope, in *Reconnection of Magnetic Fields*, edited by J. Birn and E. Priest (Cambridge University Press, Cambridge, 2007), p. 237.
- ²¹J. Heyvaerts and E. R. Priest, *Astron. Astrophys.* **117**, 220 (1983).
- ²²M. Goossens, in *Advances in Solar System Magnetohydrodynamics*, edited by E. R. Priest and A. W. Wood (Cambridge University Press, Cambridge, 1991), p. 137.
- ²³J. P. H. Goedbloed and S. Poedts, *Principles of Magnetohydrodynamics* (Cambridge University Press, Cambridge, 2004).
- ²⁴J. A. McLaughlin and A. W. Hood, *Astron. Astrophys.* **420**, 1129 (2004).
- ²⁵J. A. McLaughlin and A. W. Hood, *Astron. Astrophys.* **459**, 641 (2006).
- ²⁶M. J. Aschwanden, L. Fletcher, C. J. Schrijver, and D. Alexander, *Astrophys. J.* **520**, 880 (1999).
- ²⁷V. M. Nakariakov, L. Ofman, E. E. Deluca, B. Roberts, and J. M. Davila, *Science* **285**, 862 (1999).
- ²⁸I. De Moortel, C. E. Parnell, and A. W. Hood, *Sol. Phys.* **215**, 69 (2003).